Petroleum Science 20 (2023) 482–494

Contents lists available at ScienceDirect

Petroleum Science

journal homepage: www.keaipublishing.com/en/journals/petroleum-science

Original Paper

Pore pressure built-up in hydrate-bearing sediments during phase transition: A poromechanical approach

Shui-Tao Zhang [a, b], Lin-Lin Wang [a, b, *]

[a] State Key Laboratory of Petroleum Resources and Prospecting, China University of Petroleum (Beijing), Beijing, 102249, China
[b] Department of Offshore Oil and Gas Engineering, College of Safety and Ocean Engineering, China University of Petroleum (Beijing), Beijing, 102249, China

ARTICLE INFO

Article history:
Received 18 April 2022
Received in revised form
31 July 2022
Accepted 11 August 2022
Available online 15 August 2022

Edited by Xiu-Qiu Peng

Keywords:
Methane hydrate
Excess fluid pressure
Poromechanical
Phase equilibrium

ABSTRACT

Due to the density contrast between the hydrate and methane gas, the pore pressure is accumulated in the sediment during the decomposition process of methane hydrate. This accumulation of pore pressure decreases the magnitude of effective stress, further triggering potential geological disasters such as landslide. This paper establishes a theoretical framework to investigate the evolution of fluid pressure in the hydrate-bearing sediments during the decomposition process. This model consists of two parts: an unsaturated thermo-poromechanical constitutive law as well as a phase equilibrium equation. Compared with the existing studies, the present work incorporates the effect of pore volume change into the pressure built-up model. In addition, the capillary effect is considered, which plays a nontrivial role in fine-grained sediments. Based on this model, the evolution of fluid pressure is investigated in undrained conditions. It is shown that four mechanisms mainly contribute to the pressure built-up: the density contrast between decomposing hydrate and producing fluid, the variation of pore volume, the compaction of hydrate due to variation of capillary pressure, and the thermal deformation of pore constituents induced by temperature change. Among these mechanisms, the density contrast dominates the pore pressure accumulation. Under the combined effect of these contributions, the evolution of fluid pressure exhibits a strong nonlinearity during the decomposition process and can reach up to dozens of mega Pascal. Nevertheless, this high-level pressure built-up results in a significant tensile strain, yielding potential fracturing of the sediment.

1. Introduction

Methane hydrates are ice-like crystalline compounds in which methane molecules are trapped in the clathrate structures of water molecules (Bisio, 2007). They are stable under the condition of elevated pressure and low temperatures (Yasuhide et al., 2010; Sloan Jr and Koh, 2007) (eg. deep ocean sediments and permafrost regions (Li et al., 2013)). The total volume of methane gas trapped in the hydrate is considerable (Milkov et al., 2003; Zhang et al., 2012; Pang et al., 2021). Various methods of recovering methane gas from the hydrate are proposed, mainly based on in-situ hydrate dissociation. For example, depressurization method reduces the fluid pressure in the reservoir (Li et al., 2011; Sakamoto et al., 2007) and thermal stimulation raises the reservoir temperature (Loh et al., 2014; Fitzgerald and Castaldi, 2013) to decompose the hydrate. During the dissociation, 1 vol hydrate decomposes into 164 vol methane gas and 0.8 vol water at standard condition (273.15 K, 101 kPa). Accordingly, an excess pore pressure is built, leading to the sediment deformation and failure (Xu and Germanovich, 2006). For example, it may trigger large underwater landslides (Booth et al., 2010; Solheim et al., 2005), sediment subsidence (Chin et al., 2011), and wellbore instability (Liu et al., 2016). Hence, a precise quantification of the pore pressure build-up is of vital importance.

The evolution of pore pressure in hydrate sediments during the decomposition process involves a thermal-hydromechanical-chemical (THMC) coupling process (Liu et al., 2019a). First, the methane hydrate would decompose at certain temperature and pressure conditions. The temperature change is associated with a heat transfer process (Liu et al., 2019b, 2021), while the pressure change involves a seepage process in the porous hydrate sediment. Besides, the pore pressure is also governed by the pore volume

* Corresponding author. 18 Fuxue Road, Changping District, China.
E-mail address: linlin.wang@cup.edu.cn (L.-L. Wang).

https://doi.org/10.1016/j.petsci.2022.08.009

change, which links to the mechanical deformation. It should be noted that different processes interact each other. For instance, the phase transition is commonly accompanied with a temperature change, which leads to thermal expansion/shrinkage of the pore volume. Moreover, the induced pore pressure built-up influences in turn the phase transition and pore volume change.

All these factors should be taken into account, but most researches about pore pressure only consider of some factors. Xu and Germanovich (2006) establish a model to investigate the fluid pressure build-up in the hydrate-bearing sediments during the decomposition process, and the role of pore volume change is ignored. Kwon et al. (2008) derives a comprehensive formulation for the prediction of fluid pressure evolution in hydrate-bearing sediments subjected to thermal stimulation, but the bulk modulus is considered as a constant. Klar et al. (2013) develops a formulation of a multi-physics model of methane hydrate flow coupled to soil deformation to calculate the change of pore pressure. This model uses the phase equilibrium boundaries of methane hydrate in bulk condition to determine when the hydrate starts melt, the role of capillary effect is ignored.

This paper seeks to establish a comprehensive model to investigate the evolution of pore pressure in the sediment during hydrate decomposition process. After the introduction, the theoretical framework is proposed, including a theory of phase equilibrium and a constitutive law of unsaturated thermoporoelasticity. Based on them, the pore pressure built-up model in undrained condition is derived. In the third section, a case study of the evolution of pore pressure in undrained condition is performed, and different mechanisms contributing to the pore pressure built-up is distinguished. Afterwards, certain factors controlling the magnitude of pore pressure built-up is further discussed, including the capillary pressure, the initial hydrate saturation, and the drained bulk modulus. The last section is the conclusions.

2. Theory

2.1. Geometry description of hydrate sediments

The hydrate sediment refers to soil that accommodates hydrates. When the phase transition occurs, the hydrate decomposes into water and methane gas. In brief, hydrate sediments are composed of two types of solids (mineral grains and hydrate solid) and two liquids phases (water and gas methane). An appropriate geometry description of hydrate sediments is of crucial importance for characterizing the physical properties of such materials. In particular, the hydrate morphology is considered as a key factor controlling the mechanical and transport properties of the sediments. It is knowledged that the shape and position of hydrates is widely variable in different sediments; several hydrate habit concepts are summarized such as pore-filling, cementing, load bearing, particle-displacive etc (Waite et al., 2009; Ren et al., 2020). Accordingly, it is still an open question that regards the hydrate as solid skeleton or the pore substances. In this work, we concern the sediment behavior during the process of hydrate decomposing into water and gas. It is therefore reasonable to treat the hydrate as a pore substance. In this way, the hydrate decomposition involves simply a change of substances in the pores; it can be described by the conventional theories exploiting the phase transition phenomenons in porous media (Coussy and Monteiro, 2008).

Another challenge for the modelling is how to treat the multiple substances in the pores of hydrate sediments. Actually, the hydrate decomposition in the sediments involves a three-phases system, that is, water liquid-methane gas-hydrate solid. Nevertheless, we suggest that the gas phase exists as discontinuous bubbles dispersed within the continuous liquid phase. This configuration is suggested to be reasonable mainly based on two reasons. First, compared with liquid water, gas methane is non-wetted to solids. In other words, the gas-solid interface is unfavored, and only the liquid water wets the surface of solids (Katsuki et al., 2008). With the absence of solid-gas interface, the gas pressure can not apply on the solid (the solid skeleton and the hydrate) but transmitting through the water. Second, the water saturation in hydrate sediments is mostly larger than 50% (Terzariol et al., 2017); moreover, the emitted gas is compressed significantly under high pressure in deep ocean environment. Therefore, the volume of liquid water in pores is greatly larger than that of gas. Hence, we can reduce the three phases in the pores into two: one is the solid hydrate, the other is the fluid containing gas bubbles trapped in the water. As shown in the following, with this treatment, the gas pressure need not be considered explicitly, which would significantly simply the modelling.

Decomposition of hydrate involves an increase in fluid volume as well as a decrease in hydrate volume. Meanwhile, the pore volume can also be varied because of deformation. Hence, a relevant way to describe the volume change of fluid and hydrate is of importance. In poromechanics community (Coussy and Monteiro, 2008), the Lagrangian porosity is commonly employed, defined as the current pore volume (V_p) in reference to the initial volume of sediment (V_0).

$$\phi = \frac{V_p}{V_0} \tag{1}$$

Using the Lagrangian porosity, the change of pore volume can be simply written simply as $(\phi - \phi_0)V_0$, where $\phi - \phi_0$ is the porosity change denoted as φ. Similarly, ϕ_h and ϕ_f represent current Lagrangian partial porosities of hydrate and of fluid, with $\phi = \phi_h + \phi_f$.

The change of partial porosity during the hydrate dissociation process is attributed to two mechanisms. The first is the hydrate recession process due to hydrate dissociation without any deformation, whereas the second is related to the deformation of pores (Fig. 1). From the viewpoint of thermodynamics, this first process is governed by the change of the interface energy, while the second leads to a change of strain energy. To distinguish the two mechanisms, the partial porosity ϕ_J (J = h,f) can be expressed as:

$$\phi_J = \phi_0 S_J + \varphi_J \tag{2}$$

where S_J is Lagrangian saturation, defined as the volume of phase J with respect to the initial pore volume without deformation. According to the definition, Lagrangian saturation S_J only stands for the hydrate recession process. The sum of all phase saturations $S_h + S_f = 1$. We will see in the following that Eq. (2) can help to distinguish the different mechanisms controlling the pore pressure built-up.

2.2. Hydrate decomposition in the sediment

The formula of hydrate decomposition is written as:

$$CH_4 \cdot NH_2O(s) \leftrightarrow CH_4(g) + N \cdot H_2O(l) \tag{3}$$

where N is hydration number, which depends on hydrate compositions. F For methane hydrate, the hydration number (Sloan and Koh, 2007) ranges from 5.8 to 7.4; we adopt $N = 6$ in this paper.

Occurrence of reaction depends on temperature (T) and pressure (p). Broadly, the phase of hydrate is stable in the condition of high p and low T. With increasing T or decreasing p, the water-methane gas system becomes more stable, and the hydrate decomposes. Many scholars have determined the phase equilibrium

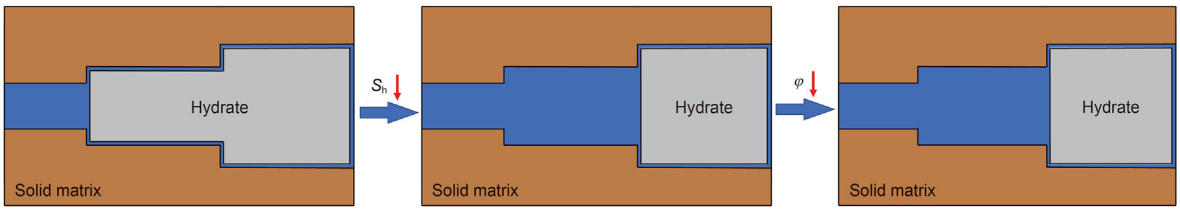

Fig. 1. Change of partial porosity during the hydrate dissociation process contains two parts: hydrate dissociation without any deformation and deformation of pores.

boundaries of methane hydrate theoretically and experimentally. In this paper, we adopt an empirical formula fitted from experimental data (Kwon et al., 2008):

$$p_{e,bulk} = \exp(40.234 - 8860/T_{e,bulk}) \tag{4}$$

where $p_{e,bulk}$ is in kPa and $T_{e,bulk}$ is in K. The subscript "bulk" indicates that Eq. (4) merely applies to the bulk condition, that is, the hydrate-water interface being flat and the hydrate pressure (p_h) equaling the fluid pressure (p_f). However, hydrate exists in the pores of the sediment. With the limited size of pores, the hydrate-water interface will be curved. This curved interface results in a pressure difference between the two sides, which is described by Laplace equation:

$$p_{nW} - p_W = \kappa\gamma, \text{with } \kappa = \frac{1}{r_1} + \frac{1}{r_2} \tag{5}$$

where γ is interface tension, and κ is the curvature of the interface. r_1 and r_2 are the principal radii of curvature. The subscripts "nW" and "W" refer to the non-wetting phase and the wetting phase, respectively. In the hydrate-fluid system, the hydrate is the non-wetting phase, and the fluid is the wetting phase.

According to the Laplace equation, the curved interface leads p_h to be higher than p_f; this pressure difference is commonly called capillary pressure (p_{hf}). Due to the capillary effect, the phase boundary of methane hydrate in the pores is shifted compared to that in the bulk condition. We derived the phase boundary of methane hydrate in the pores (Anderson et al., 2003):

$$T_{e,pore} = \left(1 - \frac{p_{hf}\overline{V}_h}{2\Delta H_{hf}}\right) T_{e,bulk} = \left(1 - \frac{\gamma_{hw}\overline{V}_h}{r\Delta H_{hf}}\right) T_{e,bulk} \tag{6}$$

where the ΔH_{hf} is the dissociation enthalpy of hydrate; its value can be considered as a constant 54.2 kJ/mol (Anderson et al., 2003). γ_{hw} is the hydrate-water interface tension equaling 32 mN/m (Yasuda et al., 2016), and r is the pore radius (in m).

However, it is important to note that Eq. (6) applies to a configuration that only the hydrate-water interface exists in the pores of sediments. Hence, the gas pressure does not emerge explicitly in the equation, and its effect is included in the term of "fluid pressure". In the preceding narrative, we have proved this configuration is reasonable.

Consider a case that the hydrate sediment locates at 200 m below the seabed with a water depth of 1200 m. The fluid pressure is accordingly 14 MPa. In such case, the melting temperature of the bulk hydrate is 288.72 K from Eq. (4) In the pores with radius of 100 nm, according to Eq. (6), the melting temperature is 288.26 K, almost the same as that in the bulk condition. However, it becomes 243.47 K in the pores of 1 nm, i.e., a shift 45.25 K compared to the bulk condition. From these calculations, we can infer that, in coarse-grain sediments (sands and silts), the capillary effect is negligible (Kwon et al., 2008). However, in fine-grained sediments, such as in the Shenhu area of the South China sea (Zhang and Cai, 2019), obvious errors would be made if we neglect the capillary effect.

According to Eq. (6), the melting temperature is reduced with decreasing pore size. The hydrate sediment contains pores with varying sizes. Thus, for a given fluid pressure, decomposition of hydrate occurs no longer at a fixed temperature but in a temperature range: the hydrate will dissociate first in small pores and then in large pores. In turn, when the temperature increases to a given value, we can calculate a critical radius r_T by Eq. (6) . The hydrate in the pores with radius smaller than r_T is decomposed, whereas the pores with radius larger than r_T is still full of the hydrate. Thus, the hydrate saturation S_h can be calculated:

$$S_h(T) = \int_0^{r_T} f(r)\mathrm{d}r \tag{7}$$

Eq. (7) implies that, at a given temperature, decomposition of hydrate or not merely depends on the pore size. Note that this is relevant for the case of hydrate decomposition but not for the formation process. Actually, formation of hydrate nucleus in bulk water is accompanied with a loss of surface energy (comparable to the supercooling phenomenon in icing). Thus, hydrate formation commonly exhibits a penetration process of a freezing front (Liu et al., 2018). This means that hydration formation process depends not only on the pore size but also on the pore connection. We take a large pore with a small entrance as an example. When temperature decreases, the large pore would freeze first but at the same temperature when the small entrance begins to freeze. However, because of disjoining pressure, a liquid film always exists between the pore wall and the hydrate. With the presence of pre-melting liquid film, the hydrate decomposition process no longer involves any loss of interface energy and can occur independently in each pores. In summary, Eq. (7) applies to the decomposition process that is not influenced by the pore connectivity.

Eq. (7) is the basis for the thermoporometry and cryoporometry methods. Both methods characterize the pore structure through measuring the ice content as a function of temperature (Sun and Scherer, 2010). In turn, once the pore size distribution of the sediment is known, the evolution of the hydrate saturation with temperature can be assessed. Considering a sediment with a pore size distribution shown in Fig. 3, the assessed variation of saturation using Eq. (6) and Eq. (7) is illustrated in Fig. 4. We can observe that the hydrate begins to decompose near 276.0 K, which is the melting temperature corresponding to the smallest pores existing in the sediment. The decomposition finally accomplishes at 289.0 K, corresponding to the melting temperature at the bulk conditions.

2.3. Unsaturated thermoporoelasticity of hydrate sediment

The hydrate decomposition has been exploited comprehensively in the previous section. The pressure built-up is not only attributed to the volume changes during the phase transition but also controlled by the variation of pore volume during the process. Hence, the constitutive law of hydrate sediment is required. The deformation of hydrate sediment during the phase transition process is a complex phenomenon, in which four main mechanisms

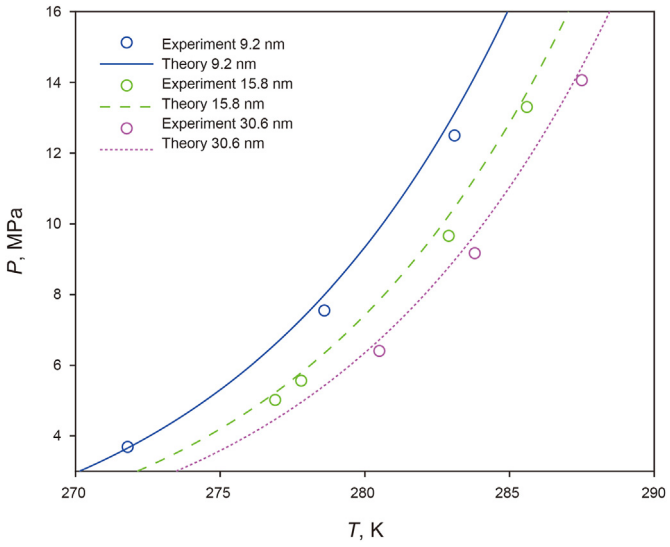

Fig. 2. Comparison of experimental data and theoretical prediction of phase equilibrium boundaries in different pore sizes.

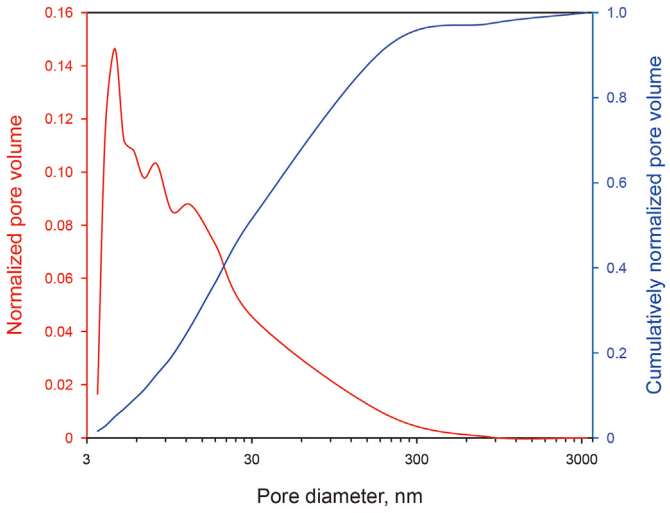

Fig. 3. Pore distribution of the hydrate sediment in Shenhu area of South China sea (Liu et al., 2012).

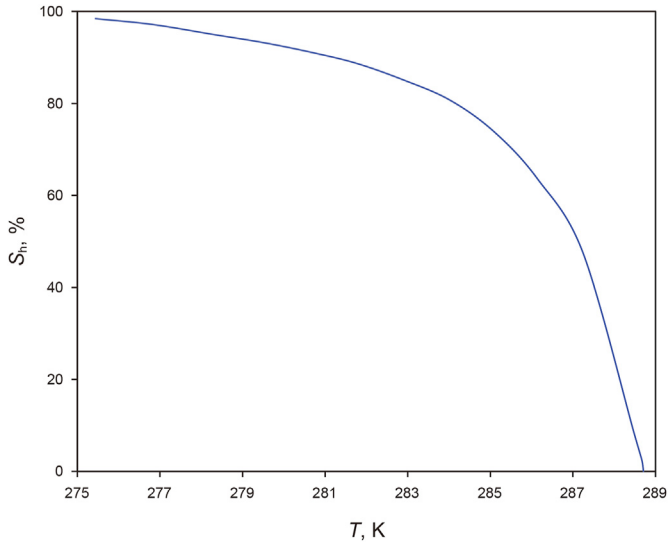

Fig. 4. Evolution of hydrate saturation with temperature at a fixed fluid pressure 14 MPa.

are involved. Besides the stress, the hydrate sediment is a porous media so the variation of the fluid pressure also contributes to the deformation. Moreover, as discussed in the previous section, the phase transition in porous media is governed by the variation of capillary pressure. We will see in the following that the variation of capillary pressure stems not only from the change of fluid pressure but also from the change of hydrate pressure. Hence, the capillary pressure, or the hydrate pressure, also leads to the deformation (Zeng et al., 2013; Zeng and Li, 2019). Finally, the phase transition is an endothermic process so is commonly accompanied with a change of temperature. The deformation induced by the change of temperature should also be considered.

The constitutive law of hydrate sediment used in the work is proposed by Coussy (Coussy and Monteiro, 2008; Wang et al., 2018). In brief, this model is established in the framework of poromechanics, which takes into account all the four mechanisms mentioned above. One key feature of this model is the way to treat the water and gas pressure. Actually, the phase transition in hydrate sediment involves three phases (solid hydrate, liquid water, and gas methane), and three pressure terms should be considered. Nevertheless, the water saturation is commonly high in hydrate sediments; moreover, the gas methane is a non-wetting phase to the solid. It is thus suggested that the gas phase exists as bubbles dispersed in the water and should not be in contact with the solid wall. Based on this configuration, the proposed model combines the two pressure (water and gas) terms into only one term called fluid pressure. With this treatment, the formula of the model can be significantly simplified. Note that the fluid pressure is already used in the formulas of phase transition based on the same consideration. The model equations are established from the thermodynamic formulation of energy conservation:

$$\begin{aligned} \mathrm{d}\sigma &= K\mathrm{d}\grave{o} - b_\mathrm{h}\mathrm{d}p_\mathrm{h} - b_\mathrm{f}\mathrm{d}p_\mathrm{f} - \beta K\mathrm{d}T \\ \mathrm{d}\varphi_\mathrm{h} &= b_\mathrm{h}\mathrm{d}\grave{o} + \frac{\mathrm{d}p_\mathrm{h}}{N_\mathrm{hh}} + \frac{\mathrm{d}p_\mathrm{f}}{N_\mathrm{hf}} - \beta_\mathrm{h}\mathrm{d}T \\ \mathrm{d}\varphi_\mathrm{f} &= b_\mathrm{f}\mathrm{d}\grave{o} + \frac{\mathrm{d}p_\mathrm{h}}{N_\mathrm{hf}} + \frac{\mathrm{d}p_\mathrm{f}}{N_\mathrm{ff}} - \beta_\mathrm{f}\mathrm{d}T \\ \mathrm{d}s_\mathrm{ij} &= 2G\mathrm{d}e_\mathrm{ij} \end{aligned} \tag{8}$$

where σ andϵ are respectively the mean stress and the volumetric strain; s_ij and e_ij the components of the deviatoric stress and the deviatoric strain tensors. K is the drained bulk modulus; G is the shear modulus.

Eq. (8) contains two pressure terms, that is, the fluid pressure (p_f) and the hydrate pressure (p_h). As used in the conventional formula of unsaturated poroelasticity, b_h and b_f are the generalized Biot coefficients for the hydrate and the fluid, respectively; N_JJ and N_hf are the generalized Biot modulus. β is the thermal volumetric dilation coefficient of the porous solid. These coefficients are related to the bulk modulus K_s and the thermal volumetric dilation coefficient of the solid matrix β_s:

$$\begin{aligned} b_\mathrm{h} + b_\mathrm{f} &= b = 1 - \frac{K}{K_\mathrm{s}} \\ \frac{1}{N_\mathrm{JJ}} + \frac{1}{N_\mathrm{hf}} &= \frac{b_\mathrm{J} - \phi_0 S_\mathrm{J}}{K_\mathrm{s}} \\ \beta &= \beta_\mathrm{s} \\ \beta_\mathrm{J} &= \beta_\mathrm{s}(b_\mathrm{J} - \phi_0 S_\mathrm{J}) \end{aligned} \tag{9}$$

With the assumption of pore volumetric isodeformation ($\phi_h/S_h = \phi_f/S_f$), b_J (J = h, f) can be expressed in a simple form:

$$b_J = bS_J \tag{10}$$

Applying Eqs. (9) and (10), the 10 coefficients in Equation finally reduce to 4: K, β_s, K_s , and G.

The hydrate sediment is commonly poorly consolidated, of which the mechanical property exhibits strong nonlinearity. For instance, the hydrate solid can bear the loading, and thus the hydrate content affects the stiffness and strength of the sediment. To consider the mechanical nonlinearity, Eq. (8) is expressed in an incremental form, and the influence of hydrate content on the stiffness is considered (Soga et al., 2010; Li et al., 2022; Zhu et al., 2021). In this present work: $K(S_h) = (100 + 450S_h)/(1 - 2\upsilon)$, $G(S_h) = (150 + 675S_h)/(1 + \upsilon)$, where K and G in MPa.

2.4. Pore pressure built-up model in undrained condition

The theory of phase equilibrium and the constitutive law of hydrate sediments are presented in the previous sections, respectively. With these two elements, the quantity of produced fluid (containing water and gas) and the variation of pore volume can be assessed during the phase transition process. Nevertheless, a pressure gradient emerges due to the induced pore pressure accumulation, leading to flows in the porous media. This transport phenomenon would diffuse the accumulated pore pressure. Accordingly, the pore pressure evolution is also governed by the transport process. In this work, we focus on an extreme condition, that is, the undrained condition. In such a condition, the transport process in totally inhibited. Hence, the magnitude of pore pressure calculated in this condition can be considered as an upper bound of the pore pressure built-up. In undrained conditions, the total mass of the substances in the pores is conserved:

$$\mathrm{d}(m_h) + \mathrm{d}\left(m_f\right) = \rho_h \mathrm{d}\phi_h \mathrm{h} + \rho_f \mathrm{d}\phi_f + \phi_h \mathrm{d}\rho_h + \phi_f \mathrm{d}\rho_f = 0 \tag{11}$$

Eq. (11) indicates that the variation in mass contents of hydrate and fluid is attributed to two part: the variation of partial porosity (ϕ_J) and the density change of each phase (ρ_J). The density changes can be expressed by the state equation:

$$\mathrm{d}\rho_J = \rho_J\left(\frac{\mathrm{d}p_J}{K_J} - \beta_J \mathrm{d}T\right) \tag{12}$$

where K_J is the bulk modulus of phaseJ. Referring to Eq. (2), the change of partial porosity contains two distinct processes: the partial saturation and the deformation of sediment. Substituting Eqs. (2) and (12) into Eq. (11) we obtain:

$$\frac{\phi_0 S_f}{K_f}\mathrm{d}p_f = -\left(\mathrm{d}\varphi_h + \mathrm{d}\varphi_f\right) + \left(1 - \frac{\rho_h}{\rho_f}\right)\phi_0 \mathrm{d}S_h - \frac{\phi_0 S_h}{K_h}\mathrm{d}p_h + \phi_0\left(S_h\beta_h + S_f\beta_f\right)\mathrm{d}T \tag{13}$$

The above equation is derived under the assumption of small deformation ($|\varphi_J| \ll 1$) and ($\left|\rho_h/\rho_f - 1\right| \ll 1$); the quadratic terms are also neglected. We can distinguish four contributions of pore pressure built-up just corresponding to the four terms in the right side of Eq. (13) . The first contribution is the pore volume change due to deformation. The minus sign in the first term indicates an increase of pore pressure with a reduction in the pore volume. The second mechanism is the density contrast between the decomposing hydrate and the producing fluid during the phase transition. If ρ_h is larger than ρ_f, the pore pressure would be accumulated with decreasing S_h. The third term corresponds to the compaction of fluid due to the hydrate pressure. As discussed previously, the hydrate decomposition in porous media is accompanied with a reduction in the capillary pressure (p_{hf}). We will see in the following that this reduction of capillary pressure is mainly achieved by an increase in the hydrate pressure. The increase of hydrate pressure would compact the hydrate, leading a negative influence to the fluid pressure built-up. The final mechanism is the dilatation of both hydrate and fluid with increasing temperature.

The variation of pore volume can be calculated from the constitutive law. In the deep sea, the geostress holds constant ($\mathrm{d}\sigma = 0$). Using Eq. (8) we can get (also consider Eq. (10):

$$\mathrm{d}\varphi_h + \mathrm{d}\varphi_f = \frac{b^2 S_h}{K}\mathrm{d}p_{hf} + \left(\frac{1}{N_{hh}} + \frac{1}{N_{hf}}\right)\mathrm{d}p_h + \left(\frac{b^2}{K} + \frac{1}{N_{ff}} + \frac{1}{N_{hf}}\right)\mathrm{d}p_f - \left(\beta_h + \beta_f - b\beta_s\right)\mathrm{d}T \tag{14}$$

Substituting Eq. (14) into Eq. (13) we finally obtain the fluid pressure equation:

$$\begin{aligned}
\mathrm{d}p_f &= \mathrm{d}p_{f1} + \mathrm{d}p_{f2} + \mathrm{d}p_{f3} \\
\mathrm{d}p_{f1} &= \frac{KM}{K_u}\left(1 - \frac{\rho_h}{\rho_f}\right)\phi_0 \mathrm{d}S_h \\
\mathrm{d}p_{f2} &= -\frac{KM}{K_u}\left(\frac{1}{M_h} + \frac{b^2 S_h}{K}\right)\mathrm{d}p_{hf} \\
\mathrm{d}p_{f3} &= \frac{KM\phi_0}{K_u}\left(S_h\beta_h + S_f\beta_f - \beta_s\right)\mathrm{d}T
\end{aligned} \tag{15}$$

where $1/M_J = 1/N_{JJ} + 1/N_{hf} + \phi_0 S_J/K_J$, $1/M = 1/M_h + 1/M_f$, $K_u = K + b^2 M$ is the undrained bulk modulus of hydrate sediment.

Eq. (15) contains three terms can be shown as Fig. 5. Referring to Eq. (13), the first term corresponds to the second mechanism mentioned previously, that is, the density difference between fluid and hydrate during the phase transition. The second term is related to the deformation under hydrate pressure (even it is written in the term of capillary pressure in the equation for the simplification of the coefficient). The variation of hydrate pressure contributes to two types of deformation: the variation of pore volume (the first mechanism) as well as the compaction of hydrate itself (the third mechanism). The third term is associated with the temperature effect that also involves two types of pressure built-up mechanisms: the thermal expansion of pore volume (the first mechanism) and the thermal expansion of hydrate and fluid (the fourth mechanism).

2.5. Physical properties of fluids

Eq. (15) contains physical properties of fluid (K_f, ρ_f, and β_f) that should be determined first. As discussed previously, the fluid here refers to a continuous water phases dispersed with gas bubbles. Therefore, K_f and β_f can be expressed by the coefficients of gas and water, respectively:

$$\frac{1}{K_f} = \frac{x}{K_g} + \frac{(1-x)}{K_w} \tag{16}$$

$$\beta_f = x\beta_g + (1-x)\beta_w \tag{17}$$

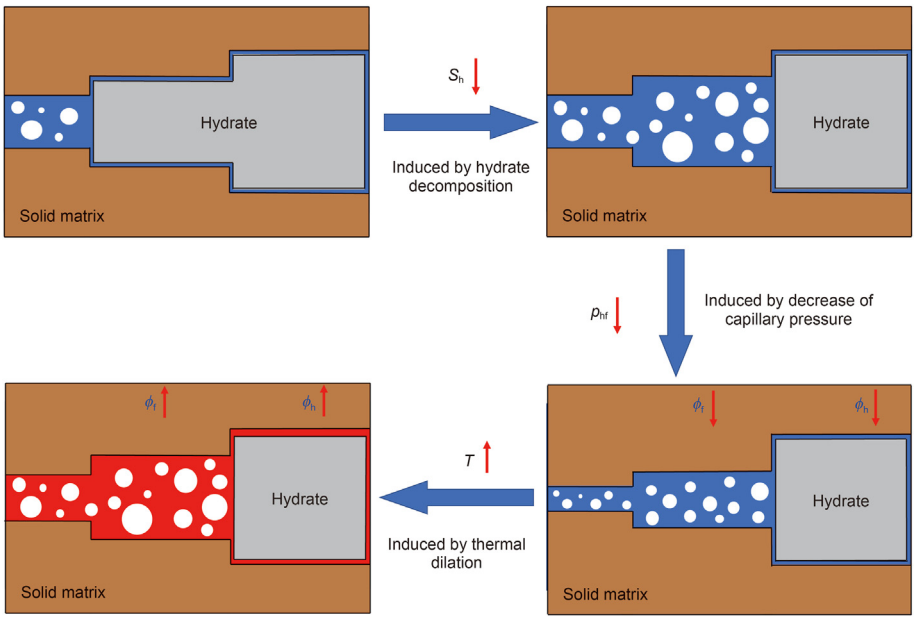

Fig. 5. Mechanism of the excess fluid pressure.

where x is the volume fraction of methane gas. Water is poorly compressible, and its bulk modulus can be considered as a constant, $K_w = 2174$ MPa (Petrenko and Whitworth, 1999). The thermal dilatation coefficient of water, β_w, depends on temperature (Kell, 1975):

$$\beta_w = 1.473 \times 10^{-9} T^3 - 1.421 \times 10^{-6} T^2 + 4.641 \times 10^{-4} T - 5.083 \times 10^{-2} \left(K^{-1}\right) \tag{18}$$

Gas methane is highly compressible, and its bulk modulus K_g and thermal dilatation coefficient β_g can be determined from its state equation:

$$p_g v_g = Z n_g R T \tag{19}$$

where v_g is gas volume, and p_g is gas pressure. n_g is the mole number of gas, and R is the gas constant with a value of 8.314 J/(mol·K). Z is the gas compression factor which can be obtained by the Standing-Katz Chart calculated by Dranchuk and Abou-Kassem (1975).

164 m^3 methane and 0.8 m^3 water is produced when 1 m^3 hydrate melt. Considering the state Eqs. (12) and (19), the volume of water and methane from melting hydrate can be calculated in virtual condition. And the fluid volume vf can be calculated by sum of the volume of water and methane. The total fluid mass mf consists of two parts: the initial water mass, the mass of produced water and gas during phase transition. The latter also equals the decomposed hydrate mass. Hence, the density of fluid can be calculated fromits definition: $\rho_f = m_f / v_f$.

3. Results and analysis

The previous section has established a model of pressure built-up during the phase transition under undrained conditions. The present section will give rise to a further analysis of this phenomenon through a case study; the main controlling factors will also be investigated. We consider a hydrate sediment that locates 200 m below the seabed with a depth of 1200 m. Accordingly, the initial fluid pressure is 14 MPa. The initial temperature is chosen as 275 K. This relative low T_0 ensures the initial condition in the pre-dissociation zone, allowing a full study of pressure built-up in the pre-dissociation, dissociation, post-dissociation regimes. The pore distribution is chosen from that shown in Fig. 2. The initial saturation of hydrate is assumed as $S_{h0} = 0.75$. Referring to Fig. 7, this initial hydrate saturation corresponds to a capillary pressure of 6.5 MPa. The physical properties of the sediment are provided in Table 1. The hydrate sediment is subjected to a step-heating in undrained conditions. The step-heating implies that the hydrate-fluid system is always in equilibrium state for each infinitesimal temperature rise.

The coefficients ρ_f, S_h,K_f in Eq. (15) depend on T. Hence, the pressure built-up model is a nonlinear problem and calculated in a

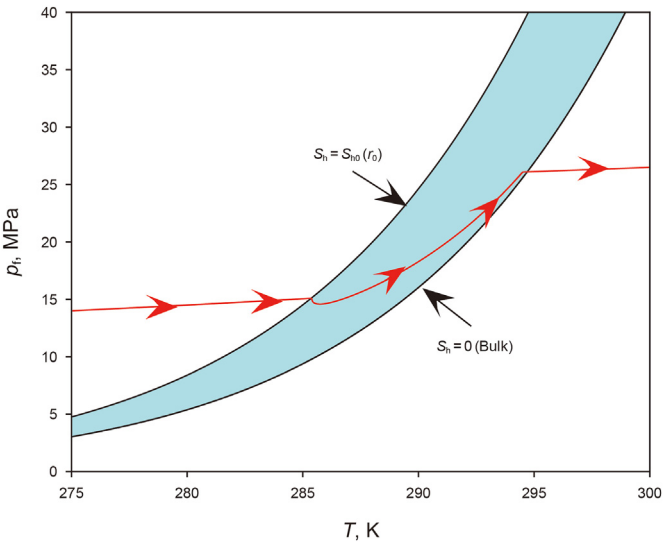

Fig. 6. Phase diagram of methane hydrate in the sediment. The phase equilibrium is shown in the diagram as a zone rather a line. The upper boundary corresponds to the smallest hydrate-occupying pores (i.e., largest water-occupying pores) at the initial saturation state. The lower boundary is the equilibrium line at the bulk condition.

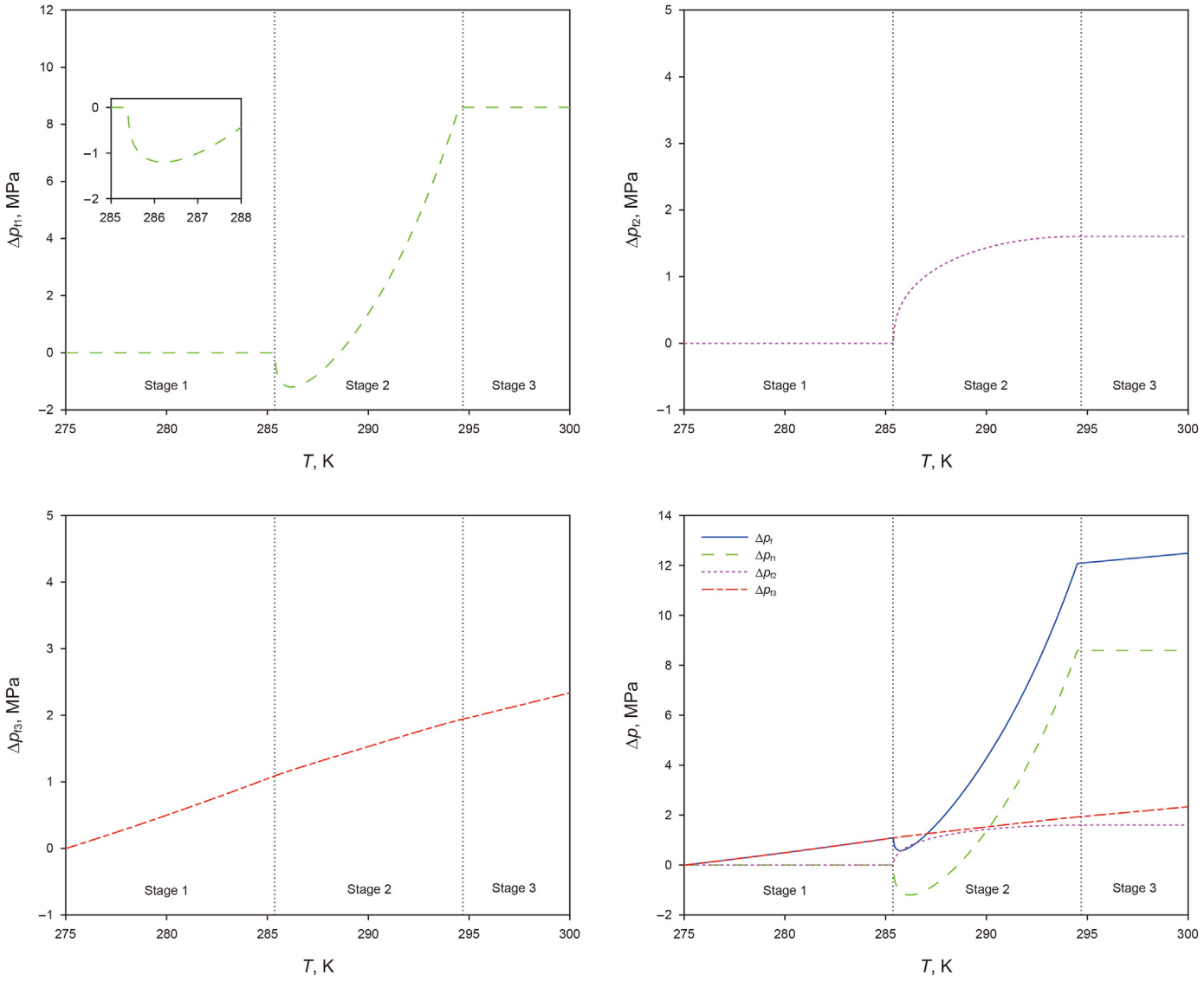

Fig. 7. Evolution of pressure built-up.

Table 1
Parameters used in calculations.

Parameter	Value	Unit	Significance
φ_0	0.38	–	Initial porosity of hydrate sediment (Zhang et al., 2010a)
S_{h0}	0.75	–	Initial hydrate saturation
p_{f0}	14	MPa	Initial fluid pressure
T_0	275	K	Initial reservoir temperature
K_s	28875.4	MPa	Bulk modulus of solid grains (Helgerud et al., 1999)
K_w	2174	MPa	Bulk modulus of liquid water (Petrenko and Whitworth, 1999)
K_h	8760	MPa	Bulk modulus of hydrate (Huo et al., 2011)
β_g	$1/T$	K^{-1}	Thermal dilation coefficient of gas
β_h	250e-6	K^{-1}	Thermal dilation coefficient of hydrate (Ning et al., 2015)
β_s	1.8e-6	K^{-1}	Thermal dilation coefficient of solids solids (Klar et al., 2013)
ρ_g^{St}	0.717	Kg/m^3	Density of methane in standard condition (Burel et al., 2013)
ρ_h	914	Kg/m^3	Density of hydrate (Uchida et al., 2002))
T_{cr}	190.56	K	Critical temperature of methane (Kurumov et al., 1988)
p_{cr}	4.5992	MPa	Critical pressure of methane (Kurumov et al., 1988)
$\Delta H_{h,f}$	54.2	kJ/mol	Dissociation constant (Atkins, 2006)
$\overline{V}_h$	1.3567e-4	m_3/mol	Mole volume of hydrate
γ_{gw}	59.3	mN/m	Methane-water interface tension (Yasuda et al., 2016)
ν	0.35	–	Poisson's ratio (Zhang et al., 2010a)

series of temperature increments. The specific calculation process is as follows.

- Given the initial fluid pressure p_{f0}, $T_{m,bulk}$ is calculated by Eq. (4)
- The critical radius of pore r that hydrate begins to decompose is calculated by Eq. (6) for the current temperature step (considered as $T_{m,pore}$); the corresponding capillary pressure p_{hf} is evaluated from Eq. (5)
- Once the critical radius is obtained, the hydrate saturation is determined by Eq. (7), and the corresponding coefficients K, M, ρ_f and x are calculated.
- The pressure change is finally obtained using Eq. (15).

The coefficients ρ_f and x are calculated as follows. Once the current saturation is obtained, the decomposed hydrate mass (also the mole number) is assessed first, and the producing water and methane (in mole) is assessed from Eq. (3). x is accordingly updated, as well as the volume of gas and methane using the state Eqs. (12) and (19). In this paper, the solubility of methane is ignored (Docherty et al., 2006). p_g is calculated from p_w ($= p_f$) using the Laplace Eq. (5) . Considering spherical gas bubbles, the curvature is $\kappa_g = 2/r_g$, where r_g is the radius of gas bubble. The methane-water interface tension takes $\gamma_{gw} = 59.3$ mN/m. The size of bubbles is variable in natural and exhibits a statistical distribution (Yang et al., 2007). We chose here an equivalent bubble size of 100 nm, which is the mean pore size of hydrate sediment selected in this study. The density of fluid is finally evaluated from $\rho_f = m_f/v_f$.

3.1. Evolution of fluid pressure

The evolution of fluid pressure with increasing temperature is illustrated in Fig. 6. Meanwhile, the evolution of fluid pressure built-up ($\Delta p_f = p_f - p_{f0}$), as well as its three components corresponding to Eq. (15), are shown in Fig. 7. The phase diagram of methane hydrate in the studied sediments is also drawn in Fig. 6. It is observed that, the phase boundary between hydrate and fluid (water + methane gas) in the sediment exhibits a zone rather a line in the p-T diagram. This is attributed to the varying pore size in the sediment for which the melting temperature is varied. Referring to Eq. (16), the hydrate in small pores decomposes at lower temperature, and that in large pores decomposes at higher temperature. Accordingly, the upper boundary of the decomposition zone corresponds to the smallest hydrate-occupying pores (i.e., largest water-occupying pores) at the initial saturation state $S_{h0} = 0.75$, that is, 11.4 nm. The lower boundary is the equilibrium line at the bulk state (Eq. (4)). Considering this decomposition zone, the path of increasing temperature can be divided into three stages: the pre-decomposition stage, the decomposition stage, and the post-decomposition stage (Fig. 6). These three stages can be shown more evidently when drawing the evolution of hydrate saturation, shown in Fig. 8. The first stage corresponds to the temperature range from 275.0 K to 285.4 K. In this pre-decomposition stage, the hydrate saturation holds constant as the initial value 0.75. In the second stage, the hydrate saturation starts to decrease till 0 at 294.5 K. The hydrate totally disappears in the third post-decomposition stage.

3.1.1. Pre-decomposition stage

We now exploit the pressure built-up and the controlling mechanisms in the three stages, respectively. From Fig. 7, during the pre-decomposition stage, the two terms related to variations of S_h and p_{hf} are both null; the pressure built-up is merely attributed to the effect of temperature. We recall that the increasing temperature not only leads to expansions of hydrate and water but also results in a compaction of pore volume. Both contributes to a pressure built-up until 1.1 MPa at the end of this stage. Note that the hydrate pressure increases simultaneously with the fluid pressure (Fig. 9). This ensures p_{hf} to keep constant as the initial value 5.6 MPa, avoiding the onset of phase transition in this stage.

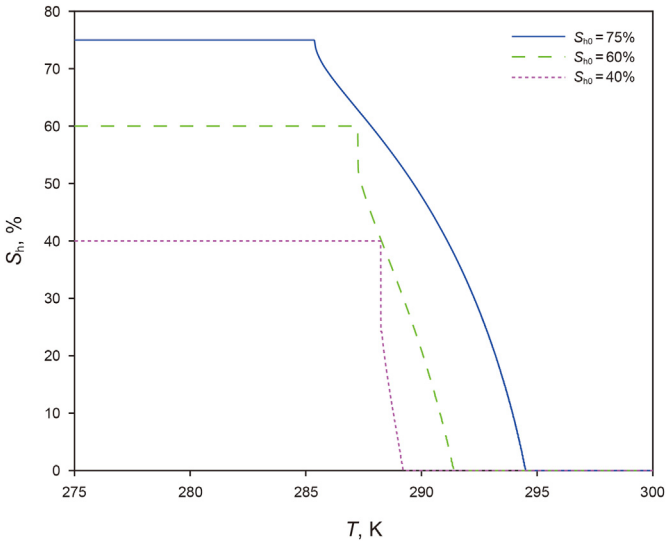

Fig. 8. Evolutions of hydrate saturation with increasing temperature.

3.1.2. Decomposition stage

During the decomposition stage, the first term of pressure built-up p_{f1} reduces first to a minimum of 1.2 MPa and then increases up to 8.6 MPa. The beginning decrease in p_{f1} can be explained by the density contrast between hydrate and fluid. As shown in Fig. 10, the hydrate density is 911 kg/m^3, while the water density is 1000 kg/m^3. Hence, the initial fluid density is large than that of hydrate, $\rho_f > \rho_h$. Once the hydrate decomposition starts, the gas methane is emitted, leading the fluid density to reduce. Nevertheless, the fluid density is still larger than that of hydrate when the amount of gas is limited. The emitted gas needs to accumulate to a threshold so that ρ_f becomes smaller than ρ_h. The threshold is $x = 11.3\%$ occurring at 286.2 K in the studied case (Fig. 10). After this density reversion, p_{f1} begins to re-increase.

The second term of pressure built-up p_{f2} increases nonlinearly from 0 to 1.6 MPa. This term is related to the deformation of porous

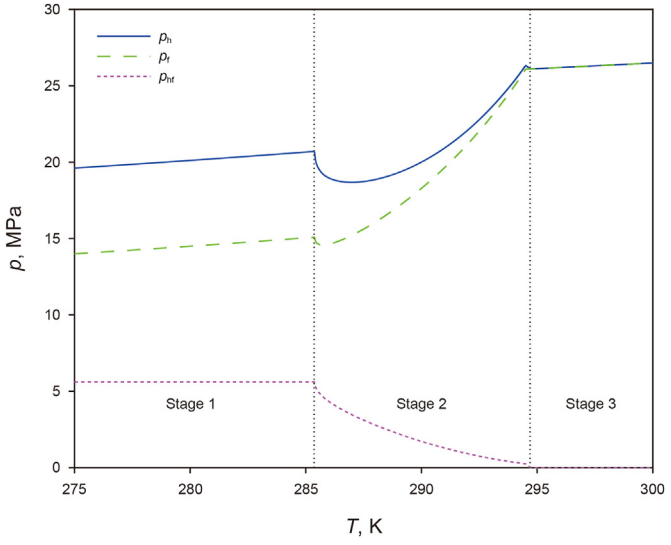

Fig. 9. Evolution of hydrate pressure, fluid pressure, and capillary pressure.

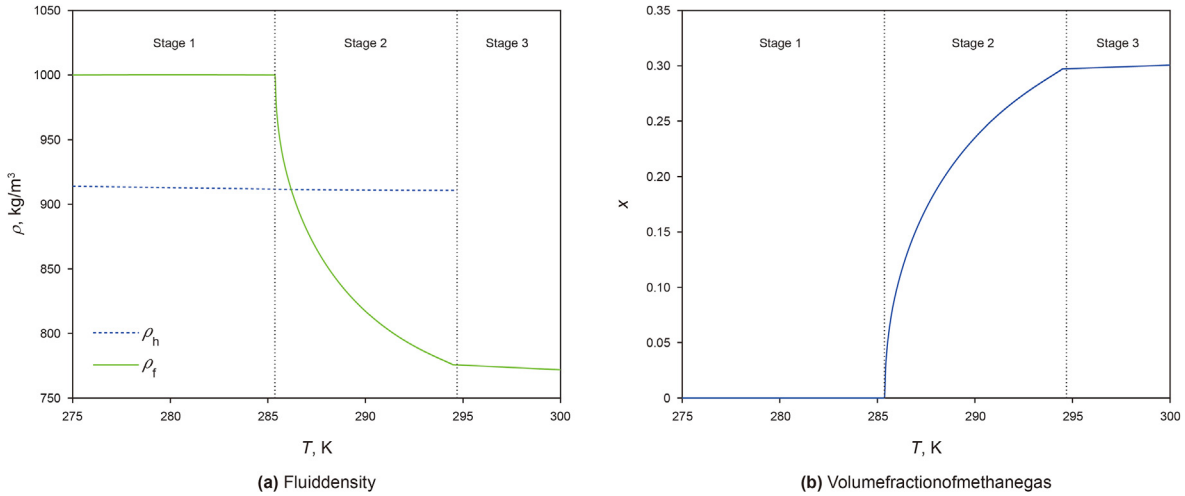

Fig. 10. Evolution of fluid density and volume fraction of methane gas during hydrate decomposition.

volume due to capillary pressure change. The third term, associated with thermal expansions of solid skeleton and pore substances, increases from 1.1 MPa to 1.9 MPa during the second stage. The total pressure built-up rises from 1.1 MPa to 12.1 MPa during the second stage. Among the three terms, the density contrast dominates the pore pressure accumulation: it contributes to 8.6 MPa, accounting for 78% of the total pressure built-up during the decomposition stage.

The first term is associated with S_h, whereas the second term is related to p_{hf}. According to Eq. (7), S_h is linked to p_{hf}. Nevertheless, the two terms are totally distinguished. We recall that S_h used in the work is Lagrangian, merely referring to the formation/decomposition of hydrate without deformation. In comparison, p_{hf} appearing in Eq. (15) corresponds to the deformation of porous volume induced by the hydrate pressure.

3.1.3. Post-decomposition stage

In the studied case, the decomposition of hydrate totally accomplishes at 294.5 K, indicating the beginning of the third stage. Similar to the first stage, the two first terms in Eq. (15) vanishes due to the absence of hydrate decomposition. The evolution of pore pressure is simply attributed to the thermal expansion, varying from 1.9 MPa at the end of the second stage to 2.3 MPa at 300 K.

In summary, the pore pressure accumulation mainly occurs in the decomposition stage: it reaches 11.0 MPa in the studied case, accounting for 88% of the total accumulation. Concerning the three contributions, the density contrast during the decomposition dominates the pore pressure built-up, accounting for 68% of the total accumulation. The second and third terms account for 13% and 19%, respectively.

The pore pressure built-up reaches up to 12.6 MPa. This significant accumulation of pore pressure is accompanied with a sharp reduction in the effective stress, leading to the deformation and potential fracturing of the sediments. More seriously, the high pore-pressure built-up might cause soil liquefaction. Note that the studied case corresponds to an undrained condition, for which the leak-off of emitted gas and water is totally inhibited. Hence, p_f evaluated in the undrained condition can be considered as the upper bound of the pressure built-up.

3.2. Evolution of pore volume

The variation of pore volume is one main mechanism governing the evolution of pore pressure. Without the total stress change, the porosity change stems from three mechanisms according to Eq. (14): 1) variation of fluid pressure, 2) variation of hydrate pressure, and 3) thermal expansions of fluid, hydrate and solid skeleton with increasing temperature. We illustrate the evolution of porosity as well as the three contributions in Fig. 11. Recall that the Lagrangian porosity used in this work describes only the changes in pore volume, excluding the change of porosity due to global deformation. From Fig. 11, the evolution of porosity can also be distinguished into three stages. It decreases to −0.24% during the pre-decomposition stage. Within the decomposition stage, the porosity decreases first and then increases up to −0.09%. The porosity continues to reduce in the post-decomposition stage; it reaches −0.76% at 300 K.

The nonlinearity exhibited in the evolution of porosity is a summing result of the three competition mechanisms. The compaction of pore volume in the first stage is mainly attributed to the thermal deformation term. This term (0.31%) is offset by the expansions by the increases in the fluid pressure (0.02%) and the hydrate pressure (0.05%). During the second stage, the thermal deformation term continues to reduce the porosity (-1.34%). However, this compaction is almost entirely offset by the significant pressure built-up leading to a pore expansion of (1.04%). Comparing

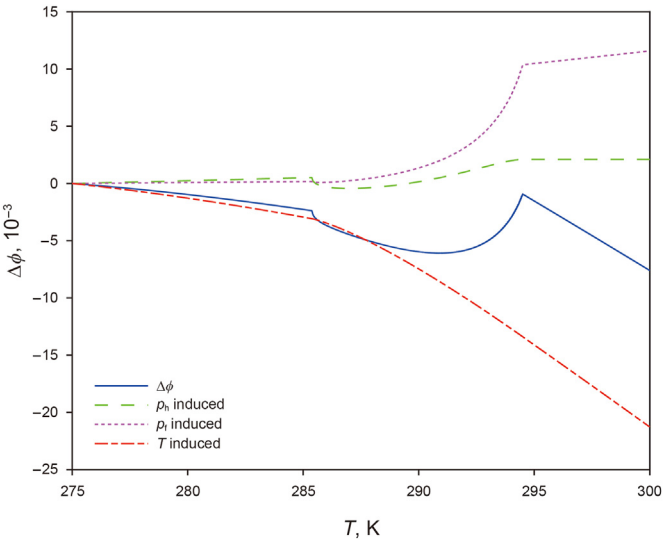

Fig. 11. Evolution of porosity with increasing temperature at undrained condition.

with these two terms, the effect of hydrate pressure is secondary, contributing only 0.21% at the end of second stage. During the third stage, the hydrate totally decomposes, and its effect vanishes. The moderate fluid pressure increase results in a slight expansion, reaching 1.16% at 300 K. The thermal deformation term reaches −2.13% at the end of third stage. In summary, the thermal deformation dominates the variation of pore volume. Nevertheless, the built-up of fluid pressure also contributes to a reverse effect in a great extent.

The existing investigations of pore-pressure built-up mostly assumed an unchanged pore volume (add two references). To quantify the effect of pore volume change, the exess pore pressure in case of $\Delta\varphi = 0$ is calculated and illustrated in Fig. 12. It is shown that, when neglecting the pore volume change, the excess pore pressure would be 0 MPa at the end of pre-decomposition stage. It rises to 5.8 MPa when hydrate is totally decomposed at 294.6 K and finally attains 6.6 MPa at 300K. In comparison, the final pressure built-up when considering the pore volume change is 12.5 MPa, nearly two times of the rigid pore volume case. Therefore, we can conclude that the volume change can not be neglected.

3.3. Evolution of deformation

One main consequence induced by the built-up of fluid pressure is the reduction in effective stress, which leads to deformation and further fracturing of the sediment. The evolution of deformation is illustrated in Fig. 13. Similar to the porosity change, the deformation is also attributed to three mechanisms according to Eq. (8): 1) variation of fluid pressure, 2) variation of hydrate pressure, and 3) thermal expansions of solid skeleton with increasing temperature. From Fig. 13, the contribution of fluid pressure dominates the deformation of sediment, followed by the effect of hydrate pressure. Different from the key role in the porosity change, the thermal dilatation term is negligible for the sediment deformation. This is mainly because the porosity change is attributed not only to the thermal expansion of solid skeleton but also those of fluid and hydrate (Eq. (14)), whereas the sediment deformation is only governed by the former (Eq. (8)). The thermal dilatation coefficient of solid skeleton is much smaller than those of hydrate and fluids (Table 1).

With the combined effect of the three mechanisms, the sediment deformation with increasing temperature exhibits nonlinearity, which can be divided into three stages. The deformation is tensile and reaches 0.07% at the end of the first stage. When the hydrate decomposes, the deformation decreases slightly first but then rises sharply up to 1.26% at the end of second stage. The deformation continues to increase during the third stage and finally reaches 1.38%. This high-level tensile strain yields geological issues such as fracturing of sediment and submarine slides (Zhang et al., 2010b).

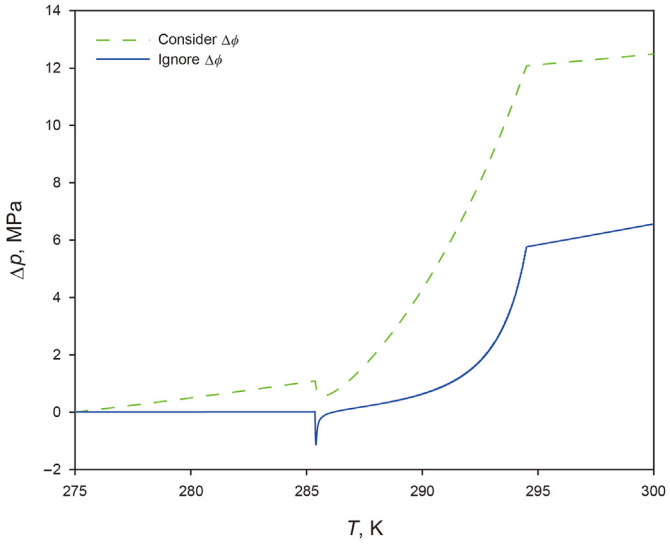

Fig. 12. Role of porosity on the pressure built-up at undrained condition.

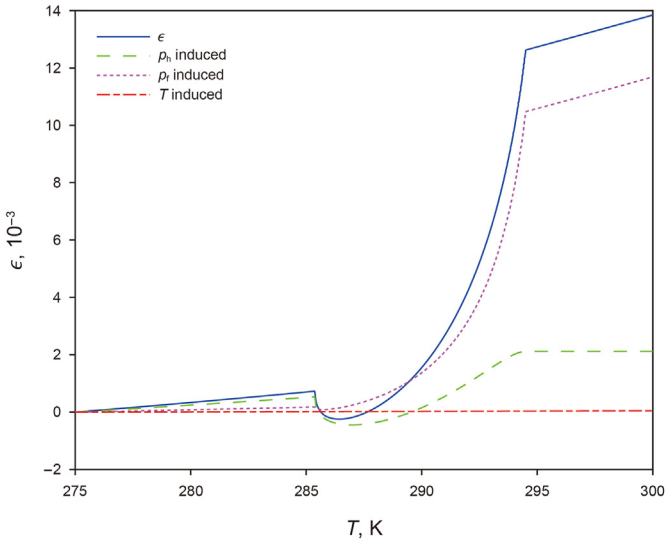

Fig. 13. Evolution of volume strain with increasing temperature at undrained condition.

4. Further discussions

4.1. Role of capillary effect

The capillary effect is considered in the present work. This effect is more obvious in fine-grained sediments, in which nanometric pores are abundant. However, the capillary effect is negligible in coarse-grained sediments. To exploit the role of capillary effect, the evolution of fluid pressure when neglecting the capillary pressure is compared with the case considering the capillary pressure, shown in Fig. 14. The two curves superpose at the beginning. Afterwards, the curve considering the capillary effect enters into the second decomposition stage in the temperature range between 285.4 K and 294.5 K. However, when neglecting the capillary effect, the evolution of fluid pressure undergoes a leap at 293.9 K, indicating the stage of hydrate decomposition.

This difference is mainly attributed to the influence of capillary pressure on the phase transition process. In coarse-grained sediments, the capillary effect is negligible so that the hydrate in all pores decomposes as in the bulk condition. For the studied case, this occurs when T reaches 293.9 K and p_f increases to 15.8 MPa according to Eq. (4). However, in fine-grained sediments, the capillary pressure leads the hydrate to decompose gradually from small pores to big pores (Eq. (6). Hence, the phase transition occurs in a temperature range for fine-grained sediments. The temperature 294.5 K at the end of decomposition is higher than 293.9 K when neglecting the capillary effect because the pressure accumulates during the decomposition process in small pores.

The final fluid pressure at 300 K is 25.8 MPa in case of neglecting the capillary effect, which is a little smaller than 26.5 MPa in case of considering the capillary effect. This is mainly due to the hydrate pressure. With the presence of capillary effect, the hydrate pressure

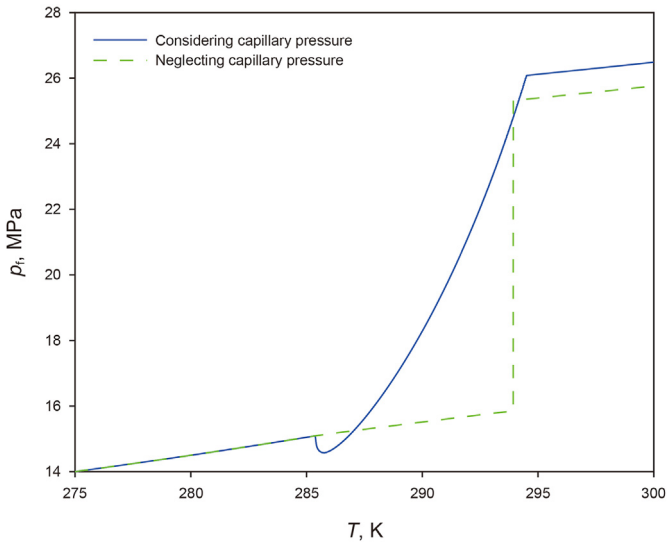

Fig. 14. Role of capillary effect on the pressure built-up.

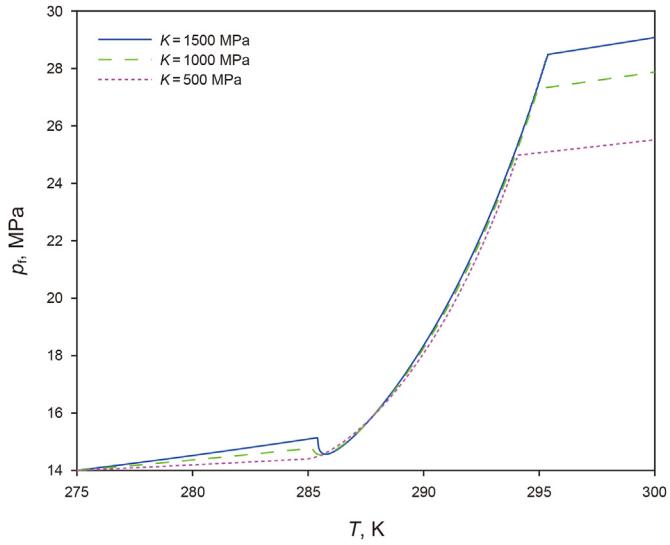

Fig. 16. Evolution of fluid pressure built-up in three cases of bulk modulus.

varies during the decomposition process, causing an additional contribution (i.e., the second term in Eq. (15)).

4.2. Influence of initial hydrate saturation

From the previous discussions, we can summarize that the fluid pressure built-up mainly stems from two terms: the density contrast between the fluid and hydrate during the phase transition process, and the variation of pore volume. We accordingly deduce that the initial hydrate saturation and the bulk modulus should be two key factors governing the pressure accumulation, which will be investigated in the two following sections respectively.

We vary the initial hydrate saturation in the studied case and calculate the final pressure built-up at 300 K, shown in Fig. 15. It is found that with increasing initial hydrate saturation, the final pressure built-up first decreases slightly and then increases up to 12.5 MPa when S_{h0} attaining 75%.

The density difference between hydrate and equivalent fluid is the main reason of this trend. In the sediment with higher initial hydrate saturation (e.g. $S_{h0} = 75\%$), the change of fluid pressure during the decomposition process can be divided into two stages: it slightly drops at the beginning and then increases. As discussed previously, the density of water is larger than that of hydrate. When only a little amount of hydrate decomposes, the density of fluid is still larger than that of hydrate, leading the fluid pressure to drop. This density contrast reverses when the emitted gas attains a threshold ($x = 11.3\%$) in the studied case from Fig. 10. To attain this threshold, less hydrate needs to decompose for low initial water saturation (i.e., high S_{h0}), whereas more hydrate needs to decompose for high initial water saturation (i.e., low S_{h0}). For an extreme case, when S_{h0} is too small, the threshold is not attained even if the hydrate totally decomposes. In other words, in the sediment with lower initial hydrate saturation, the amount of released gas from the melting hydrate is too small to reduce ρ_f smaller than ρ_h. Accordingly, the fluid pressure decreases continuously during the decomposition process. According to Eq. (15), because $\left(1 - \frac{\rho_h}{\rho_f}\right) > 0$, this paper found that with the increase of the initial hydrate saturation when $S_{h0} < 15\%$, the fluid pressure increases.

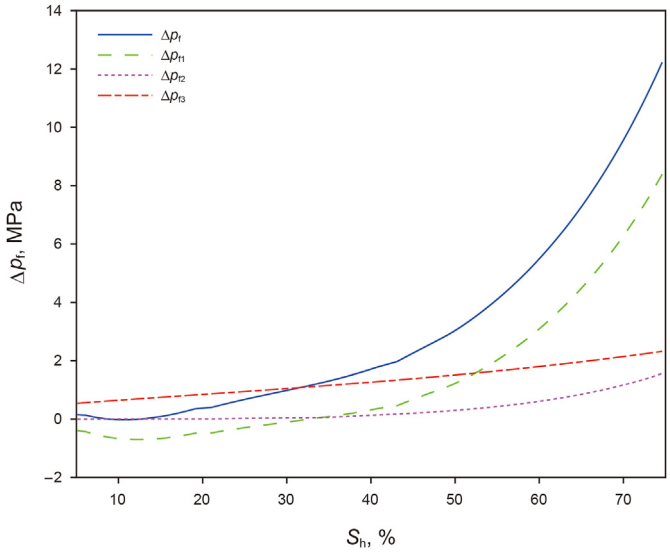

Fig. 15. Influence of initial hydrate saturation on the built-up of fluid pressure.

4.3. Influence of drained bulk modulus

As shown in Fig. 16, during hydrate recovery process, the build-up of the fluid pressure p_f increases with the increase of the drained bulk modulus (K). When $K = 1500$ MPa, the finally pore pressure is 3.6 MPa higger than $K = 500$ MPa. This is because in the sediment with lower drained bulk modulus, the increase of the pore volume is larger when rise same pore pressure. Hence, the gas from the melting hydrate has more storage space, resulting in a lower build-up pressure compared to a sediment with a larger drained bulk modulus.

When $K = 100$ MPa, the hydrate enters into the second decomposition stage in the temperature range between 284.9 K and 294.1 K. If $K = 1500$ MPa, it's found that both of the begin of hydrate decomposition temperature 285.4 K and the end of melt temperature 295.4 K is higher than when $K = 500$ MPa.This appearance can be explained in Fig. 6. In the condition of higher pressure, higher temperature is needed when hydrate begin to melt.

5. Conclusions

This paper establishes a theoretical framework to investigate the evolution of fluid pressure in the hydrate-bearing sediments during

the phase transition process. The framework consists of an unsaturated thermo-poromechanical constitutive law and a phase equilibrium theory. From this work, we can gain the following conclusions:

- When the hydrate is decomposed by thermal stimulation in undrained conditions, the fluid pressure is accumulated through a combination of several mechanisms: the density difference between hydrate and equivalent fluid (gas and water), the change of pore volume due to hydrate pressure change, and thermal expansions of fluid, hydrate and solid skeleton. Among these mechanisms, the released gas from the melting hydrate reduces the fluid density and is the main contribution of fluid pressure built-up. Since the density of water is larger than that of hydrate, the density contrast between the fluid and hydrate is first larger than 1 when a limited gas is emitted and then becomes smaller than 1 when the gas emits sufficiently. Accordingly, the corresponding pressure term drops slightly before the sharp increase. When the phase transition is absent (i.e., for the pre and post decomposition stages), the evolution of fluid pressure is mainly attributed to the thermal expansions.
- The existing investigations of excess pore pressure mostly assume a rigid pore. However, the present work demonstrates that the effect of pore volume change can't be neglected. For the studied case, the pressure built-up considering the pore volume change is twice of that considering a rigid pore.
- Under the combined effect of these mechanisms, the evolution of fluid pressure exhibits a strong nonlinearity. The built-up of fluid pressure can reach up dozens of MPa. This high-level pressure accumulation results in a sharp decrease in the effective stress. Accordingly, tensile deformation is produced, as well as potential fracturing of the sediments. More seriously, the pressure accumulation might cause geological disasters such as soil liquefaction.
- The capillary effect is negligible in coarse-grained sediments; this effect however can not be neglected in fine-grained sediments. The capillary effect causes the hydrate to decompose gradually from small pores to large pores. Hence, the phase diagram becomes a zone in fine-grained sediments rather a line for the bulk condition in the p-T chart. Moreover, the hydrate pressure varies during the decomposition process, contributing to an additional term of the built-up of fluid pressure.
- The magnitude of excess fluid pressure is affected by the initial hydrate saturation. When S_h is below certain threshold value (S_h) in the studied case, the fluid pressure drops slightly when the hydrate decomposes. When exceeding this threshold, the fluid pressure is built up during the phase transition, and its value increases with S_h. Moreover, the pressure built-up increases with the drained bulk modulus.
- The results and discussions in this work focus on the case when the hydrate decomposes by thermal stimulation in undrained condition. The value evaluated in such case can be considered as the upper bound of the pressure built-up involved in other cases. Furthermore, the theoretical framework established can be simply implemented to investigate the pressure built-up on other more realistic cases.

Acknowledgements

The authors acknowledge that this work was supported by National Natural Science Foundation of China (U20B6005).

References

Anderson, R., Llamedo, M., Tohidi, B., Burgass, R.W., 2003. Characteristics of clathrate hydrate equilibria in mesopores and interpretation of experimental data. J. Phys. Chem. B 107 (15), 3500–3506. https://doi.org/10.1021/jp0263368.
Atkins, P., 2006. Paula J. atkins' physical chemistry.
Bisio, A., 2007. Clathrate Hydrates of Natural Gases.
Booth, J.S., Winters, W.J., Dillon, W.P., 2010. Circumstantial evidence of gas hydrate and slope failure associations on the United States Atlantic continental margin. Ann. N. Y. Acad. Sci. 715, 487–489. https://doi.org/10.1111/j.1749-6632.1994.tb38863.x.
Burel, F., Taccani, R., Zuliani, N., 2013. Improving sustainability of maritime transport through utilization of liquefied natural gas (lng) for propulsion. Energy 57, 412–420. https://doi.org/10.1016/j.energy.2013.05.002.
Chin, L.Y., Silpngarmlert, S., Schoderbek, D.A., 2011. Subsidence prediction by coupled Modeling of Geomechanics and Reservoir Simulation for Methane Hydrate Reservoirs. American Rock Mechanics Association.
Coussy, O., Monteiro, P., 2008. Poroelastic model for concrete exposed to freezing temperatures. Cement Concr. Res. 38 (1), 40–48. https://doi.org/10.1016/j.cemconres.2007.06.006.
Docherty, H., Galindo, A., Vega, C., Sanz, E., 2006. A potential model for methane in water describing correctly the solubility of the gas and the properties of the methane hydrate. J. Chem. Phys. 125 (7), 074510. https://doi.org/10.1063/1.2335450.
Dranchuk, P., Abou-Kassem, H., 1975. Calculation of z factors for natural gases using equations of state. J. Can. Pet. Technol. 14. https://doi.org/10.2118/75-03-03.
Fitzgerald, G.C., Castaldi, M.J., 2013. Thermal stimulation based methane production from hydrate bearing quartz sediment. Ind. Eng. Chem. Res. 52 (19), 6571–6581. https://doi.org/10.1021/ie400025f.
Helgerud, M., Dvorkin, J., Nur, A., Sakai, A., Collett, T., 1999. Elastic-wave velocity in marine sediments with gas hydrates: effective medium modeling. Geophys. Res. Lett. 26 (13), 2021–2024. https://doi.org/10.1029/1999GL900421.
Huo, H., Liu, Y., Zheng, Z., Zhao, J., Jin, C., Lv, T., 2011. Mechanical and thermal properties of methane clathrate hydrates as an alternative energy resource. J. Renew. Sustain. Energy 3 (6), 063110. https://doi.org/10.1063/1.3670410.
Katsuki, D., Ohmura, R., Ebinuma, T., Narita, H., 2008. Visual observation of dissociation of methane hydrate crystals in a glass micro model:Production and transfer of methane. J. Appl. Phys. 104 (8), 083514. https://doi.org/10.1063/1.3000622.
Kell, G.S., 1975. Density, thermal expansivity, and compressibility of liquid water from 0.deg. to 150.deg. correlations and tables for atmospheric pressure and saturation reviewed and expressed on 1968 temperature scale. J. Chem. Eng. Data 20 (1), 97–105. https://doi.org/10.1021/je60064a005.
Klar, A., Uchida, S., Soga, K., Yamamoto, K., et al., 2013. Explicitly coupled thermal flow mechanical formulation for gas-hydrate sediments. SPE J. 18, 196–206. https://doi.org/10.2118/162859-PA, 02.
Kurumov, D., Olchowy, G., Sengers, J., 1988. Thermodynamic properties of methane in the critical region. Int. J. Thermophys. 9 (1), 73–84. https://doi.org/10.1007/bf00504001.
Kwon, T.H., Cho, G.C., Santamarina, J.C., 2008. Gas hydrate dissociation in sediments: pressure-temperature evolution. G-cubed 9 (3). https://doi.org/10.1029/2007GC001920.
Li, B., Li, X.S., Li, G., Jia, J.L., Feng, J.C., 2013. Measurements of water permeability in unconsolidated porous media with methane hydrate formation. Energies 6 (7), 3622–3636. https://doi.org/10.3390/en6073622.
Li, X.S., Zhang, Y., Li, G., Chen, Z.Y., Wu, H.J., 2011. Experimental investigation into the production behavior of methane hydrate in porous sediment by depressurization with a novel three-dimensional cubic hydrate simulator. Energy Fuels 25 (10), 4497–4505. https://doi.org/10.1021/ef200757g.
Li, Y., Cheng, Y.F., Yan, C.L., Wang, Z.Y., Song, L.F., 2022. Effects of creep characteristics of natural gas hydrate-bearing sediments on wellbore stability. Petrol. Sci. 19 (1), 220–233. https://doi.org/10.1016/j.petsci.2021.10.026.
Liu, C., Ye, Y., Meng, Q., He, X., Lu, H., Zhang, J., Liu, J., Yang, S., 2012. The characteristics of gas hydrates recovered from shenhu area in the south China sea. Mar. Geol. 307, 22–27. https://doi.org/10.1016/j.margeo.2012.03.004.
Liu, M., Jin, Y., Lu, Y., Chen, M., Hou, B., Chen, W., Wen, X., Yu, X., 2016. A wellbore stability model for a deviated well in a transversely isotropic formation considering poroelastic effects. Rock Mech. Rock Eng. 49 (9), 3671–3686. https://doi.org/10.1007/s00603-016-1019-8.
Liu, Y., Lu, J., Cheng, Q., Han, Z., 2019a. Geomechanics involved in gas hydrate recovery. Chin. J. Chem. Eng. v. 27 (9), 109–116. https://doi.org/10.1016/j.cjche.2019.02.015.
Liu, Z., Gong, D., Wang, L., 2021. Heat transfer with kinetic phase transition in geomaterials. Int. J. Heat Mass Tran. 167, 120826. https://doi.org/10.1016/j.ijheatmasstransfer.2020.120826.
Liu, Z., Pan, Z., Zhang, Z., Liu, P., Shang, L., Li, B., 2018. Effect of porous media and sodium dodecyl sulphate complex system on methane hydrate formation. Energy Fuels 32 (5), 5736–5749. https://doi.org/10.1021/acs.energyfuels.8b00041.
Liu, Z., Wang, L., Zhao, B., Leng, J., Zhang, G., Yang, D., 2019b. Heat transfer in sandstones at low temperature. Rock Mech. Rock Eng. 52 (1), 35–45. https://doi.org/10.1007/s00603-018-1595-x.
Loh, M., Too, J.L., Falser, S., Linga, P., Khoo, B.C., Palmer, A., 2014. Gas production from methane hydrates in a dual wellbore system. Energy Fuels 29 (1), 35–42. https://doi.org/10.1021/ef501769r.
Milkov, A.V., Claypool, G.E., Lee, Y.J., Xu, W., Dickens, G.R., Borowski, W.S., 2003. In situ methane concentrations at hydrate ridge, offshore Oregon: new constraints on the global gas hydrate inventory from an active margin. Geology 31 (10), 833–836. https://doi.org/10.1130/G19689.1.

Ning, F., Glavatskiy, K., Ji, Z., Kjelstrup, S., Vlugt, T.H., 2015. Compressibility, thermal expansion coefficient and heat capacity of ch 4 and co 2 hydrate mixtures using molecular dynamics simulations. Phys. Chem. Chem. Phys. 17 (4), 2869–2883. https://doi.org/10.1039/C4CP04212C.

Pang, X.Q., Chen, Z.H., Jia, C.Z., Wang, E.Z., Shi, H.S., Wu, Z.Y., Hu, T., Liu, K.Y., Zhao, Z.F., Pang, B.a., 2021. Evaluation and re-understanding of the global natural gas hydrate resources. Petrol. Sci. 18 (2), 323–338. https://doi.org/10.1007/s12182-021-00568-9.

Petrenko, V.F., Whitworth, R.W., 1999. Physics of Ice. OUP, Oxford.

Ren, X., Guo, Z., Ning, F., Ma, S., 2020. Permeability of hydrate-bearing sediments. Earth Sci. Rev. 202, 103100. https://doi.org/10.1016/j.earscirev.2020.103100.

Sakamoto, Y., Komai, T., Kawamura, T., Tenma, N., Yamaguchi, T., 2007. Field scale simulation for the effect of relative permeability on dissociation and gas production behavior during depressurization process of methane hydrate in marine sediments. In: ISOPE Ocean Mining and Gas Hydrates SymposiumISOPE OMS-2007.

Sloan, E.D., Koh, C.A., 2007. Clathrate Hydrates of Natural Gases. CRC press.

Soga, K., Ng, M.Y.A., Klar, A., 2010. Coupled deformation–flow analysis for methane hydrate extraction. Geotechnique 60 (10), 765–776. https://doi.org/10.1680/geot.9.p.079-3799.

Solheim, A., Bryn, P., Berg, K., Sejrup, H., Mienert, J., 2005. Ormen Lange: an Integrated Study for Safe Field Development in the Storegga Submarine Slide area.

Sun, Z., Scherer, G.W., 2010. Effect of air voids on salt scaling and internal freezing. Cement Concr. Res. 40 (2), 260–270. https://doi.org/10.1016/j.cemconres.2009.09.027.

Terzariol, M., Goldsztein, G., Santamarina, J.C., 2017. Maximum recoverable gas from hydrate bearing sediments by depressurization. Energy 141, 1622–1628. https://doi.org/10.1016/j.energy.2017.11.076.

Uchida, T., Ebinuma, T., Takeya, S., Nagao, J., Narita, H., 2002. Effects of pore sizes on dissociation temperatures and pressures of methane, carbon dioxide, and propane hydrates in porous media. J. Phys. Chem. B 106 (4), 820–826. https://doi.org/10.1021/jp012823w.

Waite, W.F., Santamarina, J.C., Cortes, D.D., Dugan, B., Yun, T.S., 2009. Physical properties of hydrate-bearing sediments. Rev. Geophys. 47 (4), 465–484. https://doi.org/10.1029/2008RG000279.

Wang, L., Vandamme, M., Pereira, J.M., Dangla, P., Espinoza, N., 2018. Permeability changes in coal seams: the role of anisotropy. Int. J. Coal Geol. 199, 52–64. https://doi.org/10.1016/j.coal.2018.09.014.

Xu, W., Germanovich, L.N., 2006. Excess pore pressure resulting from methane hydrate dissociation in marine sediments: a theoretical approach. J. Geophys. Res. Solid Earth 111 (B1). https://doi.org/10.1029/2004JB003600.

Yang, G.Q., Bing, D., Fan, L.S., 2007. Bubble formation and dynamics in gas–liquid–solid fluidization—a review. Chem. Eng. Sci. 62 (1–2), 2–27. https://doi.org/10.1016/j.ces.2006.08.021.

Yasuda, K., Mori, Y.H., Ohmura, R., 2016. Interfacial tension measurements in water-methane system at temperatures from 278.15 k to 298.15 k and pressures up to 10 mpa. Fluid Phase Equil. 413, 170–175. https://doi.org/10.1016/j.fluid.2015.10.006.

Yasuhide, S., Takeshi, K., Kuniyuki, M., Norio, T., Tsutomu, Y., George, Z., 2010. Laboratory-scale experiments of the methane hydrate dissociation process in a porous media and numerical study for the estimation of permeability in methane hydrate reservoir, 2010 J. Chem. Thermodyn. 9879–9884. https://doi.org/10.1155/2010/452326.

Zeng, Q., Fen-Chong, T., Li, K.F., 2013. Elastic behavior of saturated porous materials under undrained freezing. Acta Mech. Sin. 29 (6), 827–835. https://doi.org/10.1007/s10409-013-0082-6.

Zeng, Q., Li, K., 2019. Quasi-liquid layer on ice and its effect on the confined freezing of porous materials. Crystals 9 (5), 250. https://doi.org/10.3390/cryst9050250.

Zhang, K., Moridis, G.J., Wu, N., Li, X., Reagan, M.T., et al., 2010a. Evaluation of alternative horizontal well designs for gas production from hydrate deposits in the shenhu area, south China sea. In: International Oil and Gas Conference and Exhibition in China. Society of Petroleum Engineers. https://doi.org/10.2118/131151-MS.

Zhang, X., Lu, X., Li, Q., Yao, H., 2010b. Thermally induced evolution of phase transformations in gas hydrate sediment. Sci. China Phys. Sci. China. Phys. Mech. 53 (8), 1530–1535. https://doi.org/10.1007/s11433-010-4060-8.

Zhang, Y., Cai, J., 2019. Constant pressure decomposition characteristics of methane hydrate in sediments of the south China sea (Chinese). Scientia Sinica v 49, 136–143.

Zhang, Z.G., Wang, Y., Gao, L.F., Zhang, Y., Liu, C.S., 2012. Marine gas hydrates: future energy or environmental killer. Energy Proc. 16, 933–938. https://doi.org/10.1016/j.egypro.2012.01.149.

Zhu, H.Y., Dang, Y.K., Wang, G.R., Zhou, S.W., Fu, Q., 2021. Near-wellbore fracture initiation and propagation induced by drilling fluid invasion during solid fluidization mining of submarine nature gas hydrate sediments. Petrol. Sci. 18 (6), 1739–1752. https://doi.org/10.1016/j.petsci.2021.09.026.